

ornl

**OAK RIDGE
NATIONAL
LABORATORY**

MARTIN MARIETTA

MARTIN MARIETTA ENERGY SYSTEMS LIBRARIES



3 4456 0269061 1

ORNL/TM-10617

Transport Simulations of Ohmic Ignition Experiment—IGNITEX

N. A. Uckan
H. C. Howe

OAK RIDGE NATIONAL LABORATORY
CENTRAL RESEARCH LIBRARY
CIRCULATION SECTION
EIGHT ROOM 173
LIBRARY LOAN COPY
DO NOT TRANSFER TO ANOTHER PERSON
If you wish someone else to see this
report, send in name with report and
the library will arrange a loan.

OPERATED BY
MARTIN MARIETTA ENERGY SYSTEMS, INC.
FOR THE UNITED STATES
DEPARTMENT OF ENERGY

Printed in the United States of America. Available from
National Technical Information Service
U.S. Department of Commerce
5285 Port Royal Road, Springfield, Virginia 22161
NTIS price codes—Printed Copy: A03; Microfiche A01

This report was prepared as an account of work sponsored by an agency of the United States Government. Neither the United States Government nor any agency thereof, nor any of their employees, makes any warranty, express or implied, or assumes any legal liability or responsibility for the accuracy, completeness, or usefulness of any information, apparatus, product, or process disclosed, or represents that its use would not infringe privately owned rights. Reference herein to any specific commercial product, process, or service by trade name, trademark, manufacturer, or otherwise, does not necessarily constitute or imply its endorsement, recommendation, or favoring by the United States Government or any agency thereof. The views and opinions of authors expressed herein do not necessarily state or reflect those of the United States Government or any agency thereof.

ORNL/TM-10617
Dist. Category UC-20

Fusion Energy Division

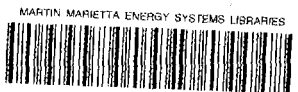
**TRANSPORT SIMULATIONS OF OHMIC IGNITION
EXPERIMENT—IGNITEX**

N. A. Uckan
H. C. Howe

Presented at the 12th Symposium on Fusion Engineering,
Monterey, California, October 12-16, 1987

DATE PUBLISHED—December 1987

Prepared by the
OAK RIDGE NATIONAL LABORATORY
Oak Ridge, Tennessee 37831
operated by
MARTIN MARIETTA ENERGY SYSTEMS, INC.
for the
U.S. DEPARTMENT OF ENERGY
under contract DE-AC05-84OR21400



3 4456 0269061 1

CONTENTS

ABSTRACT	v
1. INTRODUCTION	1
2. GLOBAL ANALYSIS	3
2.1 MODELS	3
2.2 MINIMUM REQUIREMENTS FOR OH IGNITION	5
2.3 IGNITION CONTOURS: OH + L-MODE SCALINGS	6
3. TRANSPORT SIMULATIONS WITH PROCTR	9
ACKNOWLEDGMENTS	10
REFERENCES	13

ABSTRACT

The IGNITEX device, proposed by Rosenbluth et al., is a compact, super-high-field, high-current, copper-coil tokamak envisioned to reach ignition with ohmic (OH) heating alone. Several simulations of IGNITEX were made with a 0-D global model and with the 1-D PROCTR transport code. It is shown that OH ignition is a sensitive function of the assumptions about density profile, wall reflectivity of synchrotron radiation, impurity radiation, plasma edge conditions, and additional anomalous losses. In IGNITEX, OH ignition is accessible with nearly all scalings based on favorable OH confinement (such as neo-Alcator). Also, OH ignition appears to be accessible for most (not all) L-mode scalings (such as Kaye-Goldston), provided that the density profile is not too broad (parabolic or more peaked profiles are needed), Z_{eff} is not too large (≤ 2), and anomalous radiation and alpha losses and/or other enhanced transport losses (η_i modes, edge convective energy losses, etc.) are not present. In IGNITEX, because the figure-of-merit parameters ($aB_0^2/q \sim IB_0$, etc.) are large, ignition can be accessed (either with OH heating alone or with the aid of a small amount of auxiliary power) at relatively low beta, far from stability limits. Once the plasma is ignited, thermal runaway is prevented naturally by a combination of increased synchrotron radiation, burnout of the fuel in the plasma core and replacement by thermal alphas, and the reduction in the thermal plasma confinement assumed in L-mode-like scalings.

1. INTRODUCTION

The prospect of achieving ignition in a compact, high-field, high-density, tokamak plasma has long been advocated by Coppi¹ and others.² The IGNITOR¹ and the Compact Ignition Tokamak (CIT)³ are two examples of this class of small ($R_o \sim 1\text{--}2$ m), high-power-density devices. For favorable confinement scalings, some of these ignition experiments are envisioned to reach ignition by OH heating alone.¹ Recently, to achieve OH ignition, the use of super-high fields ($B_o \sim 15\text{--}25$ T) in compact devices has been considered in the SHOT⁴ (Super High-field Ohmically heated Tokamak) and IGNITEX⁵ (IGNITION EXperiment) studies.

In this paper we examine the confinement capability of the IGNITEX device (Table 1) with a 0-D global model⁶ and with the 1-D PROCTR transport code.⁷ In addition to confirming the findings of Ref. 5, we carried out several simulations of IGNITEX plasmas to assess the sensitivity of OH ignition to assumptions about confinement scalings, plasma profiles, synchrotron radiation, impurity radiation, plasma edge conditions, and

Table 1. IGNITEX Machine and Plasma Parameters

Design Parameters ^a		
$R_o = 1.5$ m	$\kappa = 1.6$	$B_o = 20.2$ T
$a = 0.47$ m	$\delta = 0$	$I = 12$ MA
Calculated Parameters ^b		
Safety factor, $q_\psi(a)$		2.72
Elliptic cylindrical q , q_*		2.2
Density limit (10^{20} m ⁻³)		
Murakami, $\langle n_{mu} \rangle$		9.2
Greenwald, $\langle n_{GR} \rangle$		10.4
Troyon beta limit, $\beta_{crit} \approx 3I/aB_o$ (%)		3.8
Figure of merit, aB_o^2/q_*		87

^a Design parameters are specified in Ref. 5.

^b Calculated parameters: see Refs. 6 and 8 for details.

$$q_* \approx [5a(m)^2 B_o(T)/I(MA)R_o(m)][1 + \kappa^2(1 + 2\delta^2)]/2$$

$$\text{Murakami limit, } \langle n_{mu}/10^{20} \text{ m}^{-3} \rangle \approx 1.5[B_o(T)/q_*R_o(m)]$$

$$\text{Greenwald limit, } \langle n_{GR}/10^{20} \text{ m}^{-3} \rangle \approx 0.6[\kappa < J(\text{MA}/\text{m}^2) >]$$

additional anomalous losses (associated with radiation or enhanced transport processes). The physics models and assumptions used in these studies are consistent with those developed initially for the CIT by the CIT physics team and the Ignition Physics Study Group (IPSG).⁸ Results from 0-D studies are summarized in Sect. 2. Simulations with the transport code PROCTR are given in Sect. 3.

2. GLOBAL ANALYSIS

The sensitivity of OH ignition in IGNITEX plasmas to confinement assumptions, plasma profiles, and synchrotron radiation has been assessed using a simple 0-D power balance model.⁶ Direct comparisons between the global model and several radial transport code calculations (the WHIST and BALDUR codes used in connection with the CIT physics assessments^{8,9} and the PROCTR code used in this study) show good agreement over the entire range of confinement models and machine parameters covered in these studies.⁶⁻⁸ (The units used here are: mks, keV, MW, MA, with $\langle n_{20} \rangle = \langle n_e \rangle / 10^{20} \text{m}^{-3}$, $T_{10} = \langle T \rangle / 10$ keV, where $\langle n \rangle$ is the volume-averaged density and $\langle T \rangle$ is the density-weighted temperature. The average atomic mass $A_i \approx 2.5$.)

2.1 MODELS

The various terms in the power balance are evaluated considering radial profiles $X = X_0(1 - r^2/a^2)^\alpha$, where $X = n, T, J$, with $\alpha_n = 0.5-1.0$ and $\alpha_T \approx 2\alpha_J/3$. For the IGNITEX parameters (see Table 1), $q(0) \geq 1.0$ is maintained with a nearly parabolic T_e profile ($\alpha_T \approx 1.0$). Because of the high density and relatively low ignition temperatures in high-field devices, the ion and electron coupling is strong and $T_e \approx T_i \approx T$. The fuel ion mixture is 50:50 deuterium-tritium (D-T) with $Z_{\text{eff}} = 1.5$ (made up of oxygen impurity and thermal alphas). Neoclassical electrical resistivity enhancement is used to evaluate the OH power. Energetic alpha particles are included in the plasma pressure and total toroidal beta value.

Bremsstrahlung and synchrotron radiation are considered (line radiation is neglected). Synchrotron radiation is estimated from an empirical model (a "universal" approximation formula) developed by Trubnikov,¹⁰ which is given (in MW/m³) by

$$P_S \approx 1.3 \times 10^{-4} (B_0 T_{10})^{5/2} [(n_{20}/a)(1 + X)]^{1/2} (1 - \mathfrak{R})^{1/2} \quad (1)$$

where $X \approx \langle 5.7 / [(R_0/a)(T_{10})^{1/2}] \rangle$. In plasmas with very high magnetic fields and low wall reflectivity (\mathfrak{R}), this loss process could be large enough, even at low temperatures

($\langle T \rangle \sim 4\text{--}7$ keV), to prevent OH ignition. For metal surfaces, \mathfrak{R} is typically high, $\sim 90\text{--}98\%$. For carbon-covered surfaces, wall reflectivity is uncertain. A smooth carbon surface may be highly reflective ($\mathfrak{R} > 0.9$). However, corrosion and redeposition of carbon could lead to a very low reflectivity ($\mathfrak{R} \sim 0$, a perfect microwave absorber).

A combination of OH and L-mode scaling¹¹ of the form $(1/\tau_E)^2 = (1/\tau_{EOH})^2 + (1/\tau_{EL})^2$ is used. (Because there is no divertor in the IGNITEX device, H-mode confinement is not considered.) Both the OH and alpha power are included in the degradation of confinement with heating power ($P_{\text{heat}} = P_{\text{OH}} + P_{\alpha}$) in τ_{EL} . Plasma operation is limited in density, beta, and q (current) space. The limiting expressions and corresponding values are given in Table 1. The following confinement models (some of which are also used for the CIT assessments^{6–9} and in the IGNITEX study⁵) are used to illustrate the range of performance.

1. *OH Scaling* (τ_E or τ_{Ee}): Neo-Alcator-Like (NA)^{8,11}

$$\tau_{EOH} = \tau_{ENA} \approx 0.07 \langle n_{20} \rangle a R_o^2 q_* \quad (2)$$

where q_* is the value of q in an elliptical cylinder with lowest order (κ, δ) corrections (as defined in Table 1).⁶ This is an optimistic scaling law ($\tau \sim n$); it does not yield the partial ($\tau \sim n^x$ with $x < 1$) or complete ($\tau \sim n^0$) saturation of confinement observed in high-density ohmic plasmas.

2. *L-mode Scaling* (τ_E or τ_{Ee}): Kaye-Goldston (KG)^{8,11}

$$\begin{aligned} \tau_{EL} = \tau_{EKG} \approx & 0.072 I^{1.24} R_o^{1.65} \langle n_{20} \rangle^{0.26} \kappa^{0.28} \\ & \times [(P_{\text{heat}})^{0.58} a^{0.49} B_o^{0.09}]^{-1} \end{aligned} \quad (3)$$

3. *Ion Neoclassical Scaling* (χ_i ; τ_{Ei}): Chang-Hinton (CH)¹²

In the low collisionality, banana regime, $\chi_i \approx f_i \chi_{CH}$.

$$\chi_{CH} \approx 0.024 K_2^* [\langle n_{20} \rangle Z_{\text{eff}} q_*^2 / \epsilon^{3/2} \langle T_{10} \rangle^{1/2} B_o^2] [2 / (1 + \kappa^2)] \quad (4)$$

where $K_2^* \approx (0.66 + 1.88\varepsilon^{1/2} - 1.54\varepsilon)(1 + 1.5\varepsilon^2)$, $\varepsilon = r/R_0$, and $f_i \sim 1-4$ is the neoclassical multiplier.

$$4. \text{ Combined OH + L-mode: } (1/\tau_E)^2 = (1/\tau_{EOH})^2 + (1/\tau_{EL})^2$$

$$(a) \quad \tau_{Ee} \approx \tau_{Ei} \approx \tau_E \approx \tau_{KG+NA} \quad \Rightarrow \quad \chi_e \approx \chi_i \approx \chi_{KG+NA} \quad (5)$$

$$(b) \quad \tau_{Ee} \approx \tau_{KG+NA}; \tau_{Ei} = \tau_{CH}/f_i \quad \Rightarrow \quad \chi_e \approx \chi_{KG+NA}; \chi_i = f_i \chi_{CH} \quad (6)$$

where $\chi_j \approx (0.3a^2/\tau_{Ej})[2\kappa^2/(1 + \kappa^2)]g(r)$ with $j = e, i, NA, KG, \dots$, $\chi_{KG+NA} = [(\chi_{KG})^2 + (\chi_{NA})^2]^{1/2}$, and $g = [1 + 4(r/a)^2]/2$.

2.2 MINIMUM REQUIREMENTS FOR OH IGNITION

The steady-state power balance equation is $F(\langle n \rangle, \langle T \rangle) = \langle P_\alpha + P_{OH} - P_{con} - P_{rad} \rangle = 0$, where the angle brackets designate volume averages. The optimal condition for OH ignition is determined from the saddle point, $F = \partial F / \partial T = \partial F / \partial n = 0$, which is satisfied at (n^*, T^*) , requiring a minimum "figure-of-merit" parameter⁶ (such as $aB_0^2/q^* \sim IB_0$). For confinement models of the form $\tau_E \sim n^x T^y$ ($P_{con} = P_e + P_i \sim n^{1-x} T^{1-y}$), it is possible to solve the saddle point equations analytically. Such analytic solutions exist for the following two examples. For simplicity, it is assumed that synchrotron emission is negligible ($\mathfrak{X} \geq 0.95$) and $\langle \sigma v \rangle_{DT} \sim T^3$ (a good approximation for $\langle T \rangle \sim 4-8$ keV).

Example 1. Neo-Alcator-like OH scaling: Taking $\tau_{Ee} \approx \tau_{Ei} \approx \tau_{NA}$ (e.g., $\chi_e \approx \chi_i \approx \chi_{NA}$), where $x = 1$ and $y = 0$, we obtain the optimal conditions needed for OH ignition from the saddle point equations, which are $P_\alpha = P_B = P_{con} = P_{OH}$. For nominal profiles ($\alpha_n \sim 0.5-1.0$, $\alpha_T \approx 1.0$) and $Z_{eff} = 1.5$, $\langle T^* \rangle \approx 4.2$ keV and the minimum figure-of-merit parameter needed for OH ignition is $(aB_0^2/q^*)_{min-OH} \approx 74[2\kappa/(1 + \kappa^2)]^2$, which is ~ 60 for the IGNITEX geometry. In IGNITEX, $aB_0^2/q^* \approx 87$ (see Table 1). Thus, for this scaling assumption (neo-Alcator scaling with no density saturation), OH ignition is accessible in IGNITEX. OH ignition is, however, prevented if confinement is degraded by a factor $f_{NA} > 1.5$ (e.g., no OH ignition if $\chi_e \approx \chi_i > 1.5\chi_{NA}$).

Example 2. Combined neoclassical ion and neo-Alcator electron scalings: For $\chi_i = f_i \chi_{CH}$ and $\chi_e = f_{NA} \chi_{NA}$, the optimal OH ignition condition is determined from $P_\alpha = P_B + P_i = P_e = P_{OH}$. This yields $(aB_0^2/q^*)_{\min-OH} \approx c_1 [1 + (1 + 2c_2/c_1)^{1/2}]$, where (for IGNITEX-like geometry, $A \sim 3$) $c_1 \approx 20f_{NA} [2\kappa/(1 + \kappa^2)]^2$ and $c_2 \approx 17f_i/a\kappa^2$. Profile and Z_{eff} assumptions are the same as in example 1. For $f_{NA} \approx 1$ and $f_i \approx 1$, IGNITEX ignites ohmically. However, OH ignition is lost if (a) $f_i \approx 1$, $f_{NA} > 2.2$; (b) $f_i \approx 4$, $f_{NA} > 1.6$; or (c) $f_{NA} \approx 1$, $f_i > 10$.

2.3 IGNITION CONTOURS: COMBINED OH + L-MODE SCALINGS

The confinement models considered in earlier examples do not yield the saturation (at high density) or degradation (with heating power) of confinement. The combined OH plus L-mode scalings represented by Eqs. (5) and (6) incorporate these effects. Direct comparisons between the global model and the PROCTR simulations are made for the reference confinement model given by Eq. (6).

OH ignition is achieved with the reference confinement model ($\chi_e = \chi_{KG+NA}$ and $\chi_i = 4\chi_{CH}$) for both broad ($\alpha_n \approx 0.5$) and parabolic ($\alpha_n = 1$) density profiles if the wall reflectivity of synchrotron radiation is high. Ignition is prevented for the case with $\alpha_n \approx 0.5$ if the wall reflectivity is reduced below 70%. OH ignition is not recovered by lowering the χ_i multiplier to one. Figure 1 shows the ignition curves in density-temperature space for $\alpha_n = 0.5$ and 1 with $\mathfrak{R} = 0.9$ and 0. In cases where OH ignition is accessed, the saddle point (optimal path to ignition) is typically around $\langle T \rangle \sim 6$ keV and $\langle n_e \rangle \sim 5.5 \times 10^{20} \text{ m}^{-3}$, and the minimum beta at ignition is $\langle \beta_{\min} \rangle \sim 0.5\text{--}0.6\%$. There is a finite density window within which OH ignition is accessible (Fig. 1). The toroidal beta contours, including the fast-alpha pressure contribution, are given in Fig. 2. Figures 1 and 2 can be overlaid to determine the extent of the operating regime in (n - T) space.

For the case of parabolic profiles ($\alpha_n = 1$) with $\mathfrak{R} = 0.9$, ignition is prevented when the reference χ_e is enhanced by 50%, even when the χ_i multiplier is reduced to one (because $\chi_e > \chi_i$). For temperatures and densities characteristic of the OH ignition regime

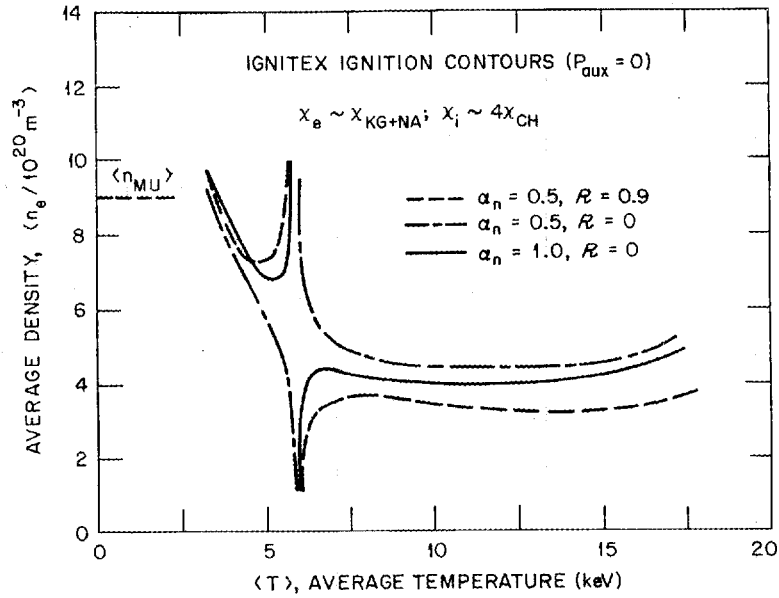


Fig. 1. Ignition contours for Kaye-Goldston + neo-Alcator electron and neoclassical (4 times Chang-Hinton) ion transport model with density profiles $\alpha_n = 0.5$ and 1.0 , $\mathfrak{R} = 0$ and 0.9 . OH ignition is accessible in all cases, except for $\mathfrak{R} = 0$, $\alpha_n = 0.5$. The ignition curve for a case (not shown) with $\mathfrak{R} = 0.8$, $\alpha_n = 1.0$ (a reference model for PROCTR simulations) is nearly identical to the curve represented by $\mathfrak{R} = 0.9$, $\alpha_n = 0.5$.

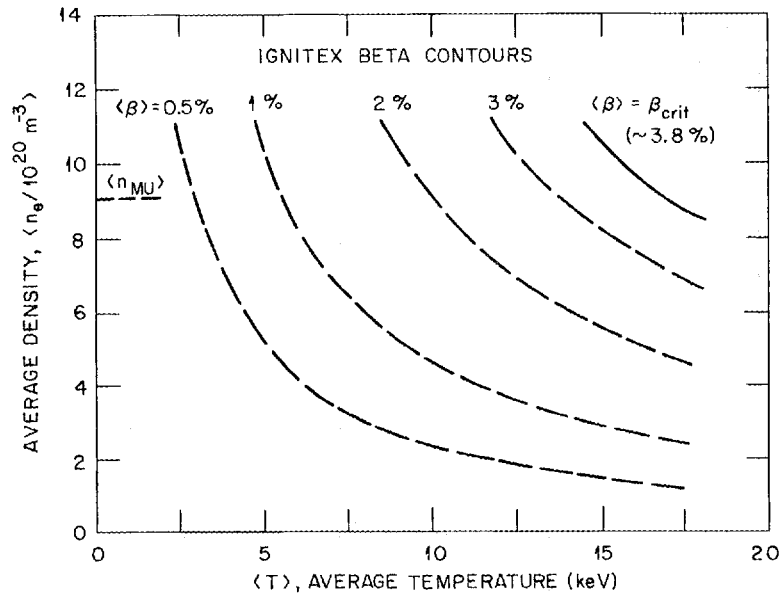


Fig. 2. Toroidal beta contours, including fast-alpha pressure contribution.

in the IGNITEX device, the neo-Alcator component of the confinement time dominates [$\chi_{\text{NA+KG}} \sim (1.2-1.4)\chi_{\text{NA}}$].

Results from a series of computational runs with the PROCTR code (with $\alpha_n = 1$) are in agreement with the global predictions (Fig. 1). Once the plasma is ignited, thermal runaway is prevented naturally by a combination of increased synchrotron radiation losses, burnout of the fuel in the plasma core and replacement by thermalized alphas, and the reduction in the thermal plasma confinement assumed in the L-mode model.

To simulate cases where the ion losses diverge from the neoclassical value ($\chi_i \geq \chi_e$), the global confinement model with $\tau_{Ee} \approx \tau_{Ei} \approx \tau_E \approx \tau_{\text{KG+NA}}$ ($\chi_e \approx \chi_i \approx \chi_{\text{KG+NA}}$), which was assumed in CIT studies,^{4,7,8} has been considered. Figure 3 shows the ignition contours for this case. OH ignition is achieved (within some density window) for $\mathfrak{R} = 0.9$ but not $\mathfrak{R} = 0$. Modest peaking of density profile (from $\alpha_n = 0.5$ to $\alpha_n = 1$) did not help to reach OH ignition for $\mathfrak{R} = 0$, as indicated in Fig. 3.

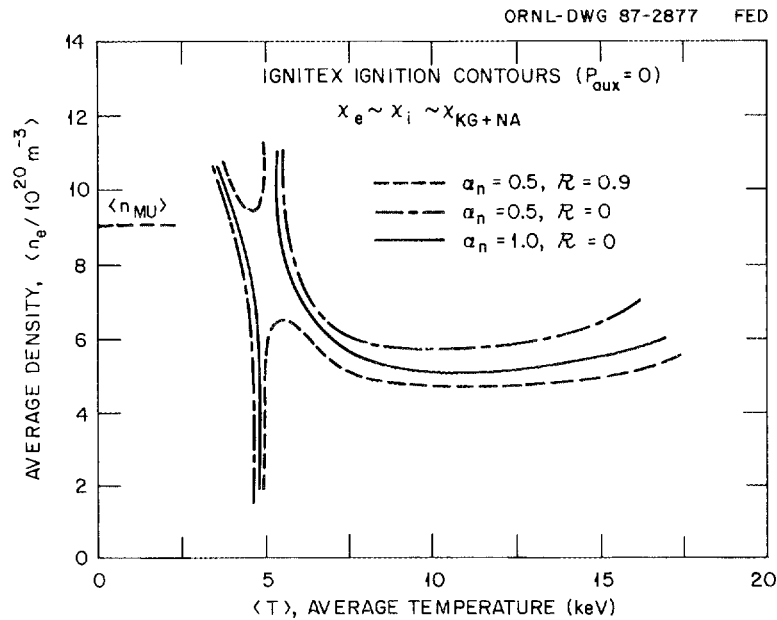


Fig. 3. Ignition contours for global Kaye-Goldston + neo-Alcator transport model ($\chi_e \approx \chi_i \approx \chi_{\text{KG+NA}}$) with square-root parabolic ($\alpha_n = 0.5$) and parabolic ($\alpha_n = 1$) density profiles. OH ignition is accessible within some density window for $\mathfrak{R} = 0.9$, but not for $\mathfrak{R} = 0$.

3. TRANSPORT SIMULATIONS WITH PROCTR

Several simulations of IGNITEX were made with the transport code PROCTR⁷ to examine the sensitivity of OH ignition to assumptions about confinement models, plasma edge conditions, and additional losses associated with anomalous radiation and enhanced transport processes. The transport model assumed electron heat conductivity χ_e given by a combination of Kaye-Goldston (L-mode) plus neo-Alcator scaling,¹¹ as described in Sect. 2. The degradation of χ_e due to heating included the ohmic and alpha heating power. The ion heat conductivity χ_i was given by the Chang-Hinton formula¹² with a multiplier of 4. Both χ_e and χ_i were enhanced by a large, arbitrary amount inside the $q_\psi = 1$ region to simulate the effect of internal disruptions. The density profile was governed by a balance between anomalous diffusivity (with the diffusion coefficient $D = 0.1 \text{ m}^2/\text{s}$) and an empirical inward convective flux that was automatically adjusted to force the density profile toward a parabolic shape ($\alpha_n \approx 1.0$). The external gas feed rates were feedback-controlled to give equal, preset volume-average deuterium and tritium densities. Plasma recycling was held below unity by assuming that all nonreflected charge-exchange neutrals were absorbed by the wall. The density of carbon was adjusted to give a plasma $Z_{\text{eff}} = 1.5$. Radiation was due primarily to bremsstrahlung and synchrotron emission¹⁰ (with $\mathfrak{R} = 0.8$). Carbon line radiation was given by coronal values and was therefore negligible. The steady-state current profile was used, and no attempt was made to model resistive decay of induced poloidal magnetic fields. The current profile was not flattened inside the region where $q_\psi < 1$ beyond the flattening of the T_e profile resulting from the χ_e enhancement.

The IGNITEX machine parameters given in Table 1 were used for the PROCTR simulations. The volume-averaged electron density was maintained by gas feedback at $\langle n_e \rangle = 4 \times 10^{20} \text{ m}^{-3}$. OH ignition was achieved with the reference L-mode χ_e and neoclassical χ_i model ($\chi_e = \chi_{\text{KG+NA}}$, $\chi_i = 4\chi_{\text{CH}}$). Ignition was prevented if twice the reference L-mode χ_e ($\chi_e = 2\chi_{\text{KG+NA}}$) was used. These results agree with the global model predictions discussed in Sect. 2 (Fig. 1) and help validate the approximations made in the model. The addition of anomalous radiation equal to 25% of the total electron heating power also

prevented ignition, even though the extra radiation was peaked in the plasma edge. Ignition was not recovered by lowering the χ_j multiplier to one or by eliminating the impurities ($Z_{\text{eff}} = 1$).

OH ignition was not obtained for the reference case with L-mode scaling when an actual limiter scrape-off (assuming a toroidal belt limiter) was included in the simulation. The particle diffusion coefficient was assumed to be $D = 1 \text{ m}^2/\text{s}$ in the scrape-off layer and $D = 0.1 \text{ m}^2/\text{s}$ in the main plasma. The resulting density profile was the same (parabolic) as in the case without scrape-off; the volume-averaged electron density was also unchanged. The presence of the scrape-off caused an increase in the amount of edge recycling and a resulting increase in the edge convective energy loss. The temperature in the outer region of the plasma was lowered by the increased convective loss, and the steep-gradient region at the plasma boundary, evident on the T_e profile in Fig. 4, was removed. The peripheral region of convection-dominated transport formed a heat sink for the plasma core that was not present in the ignited case (Fig. 5). The increase in the conductive loss from the plasma core into the cooler outer region lowered the central temperature enough to prevent ignition. The power balance for this case [Fig. 5 (bottom)] is closer to the type of edge balance typically observed in simulations of present-day tokamak experiments where the central conduction loss is linked in series to the edge convection loss such that most of the transport loss through the plasma edge is by convection rather than by conduction. From this simulation, we see that profile effects (especially those at the plasma edge), which are outside the approximations made for the 0-D model, are important in predicting OH ignition. Further, edge recycling must be taken into account when simulating ignition because edge heat sinks can have a substantial effect on the core plasma.

ACKNOWLEDGMENTS

We thank R. Carrera, M. N. Rosenbluth, and J. Sheffield for helpful discussions.

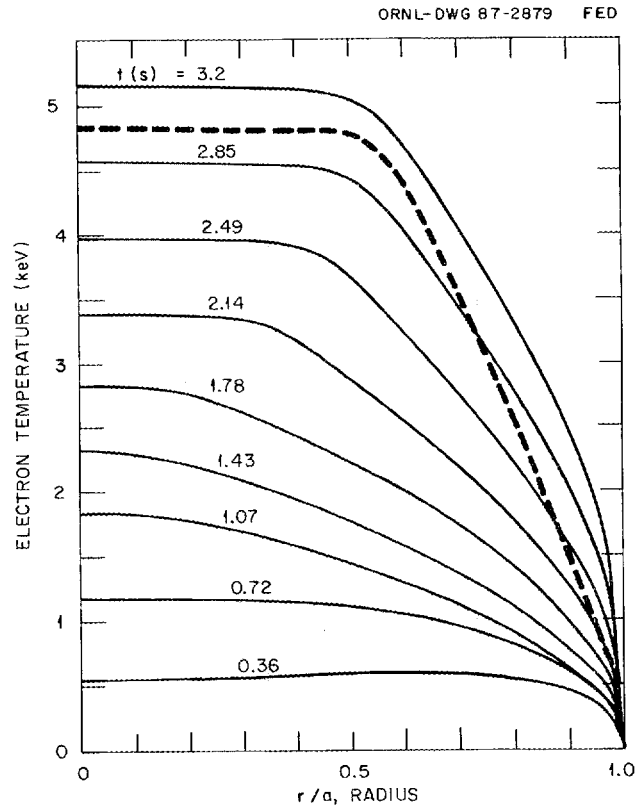


Fig. 4. Temporal evolution of the T_e profile for the ignited case (without a scrape-off layer) for times before ignition. The additional edge convective loss due to inclusion of the plasma scrape-off layer removed the steep-gradient part of the profile at the plasma edge and prevented ignition; the resulting steady-state T_e profile is shown as a dashed line.

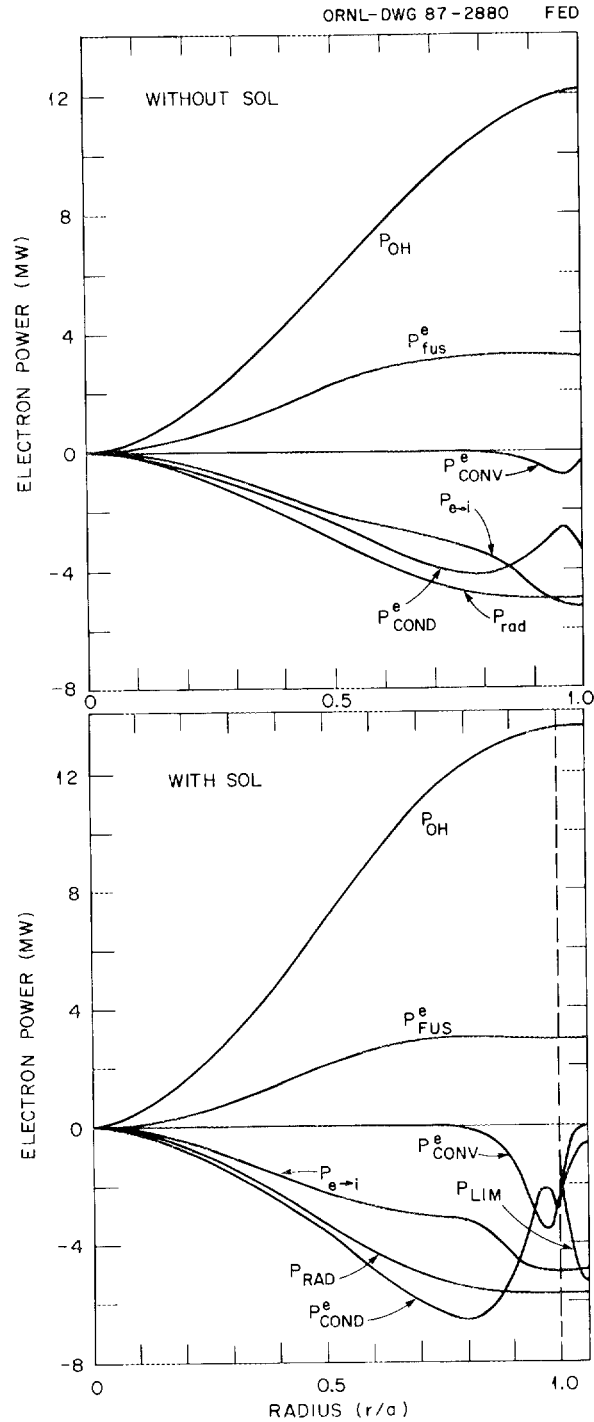


Fig. 5. Integrated electron power balance for the ignited (top) and nonignited (bottom) cases. Power balance for the ignited case is shown at time $t = 3.2$ s; see Fig. 4. The nonignited case includes the scrape-off, which results in higher recycling and larger edge convective loss P_{CONV}^e and a resulting larger conductive loss P_{COND}^e from the plasma core into the cooler edge.

REFERENCES

- [1] B. Coppi, "Compact Experiments for α -Particle Heating," *Comments Plasma Phys. Controlled Fusion*, vol. 3, pp. 47–62, 1977; "Compact Ignition Experiments: Physics and Design Issues," *Comments Plasma Phys. Controlled Fusion*, vol. 11, pp. 47–61, 1987.
- [2] D. R. Cohn et al., "Characteristics of High-Density Tokamak Ignition Reactors," *Nucl. Fusion*, vol. 16, pp. 31–6, 1976.
- [3] "CIT Conceptual Design Report," Princeton Plasma Physics Laboratory, May 1986; also see CIT papers presented at this meeting.
- [4] D. R. Cohn et al., "Super High-Field Ohmically Heated Tokamak Operation," *Fusion Technol.*, vol. 10, pp. 1111–1116, 1986.
- [5] R. Carrera, E. Montalvo, and M. N. Rosenbluth, "Ohmic Ignition in Compact Experiments," *Bull. Am. Phys. Soc.*, vol. 31, p. 1565, 1986; R. Carrera et al., "Fusion Ignition Experiment (IGNITEX)," these proceedings.
- [6] N. A. Uckan, "A Simple Procedure for Establishing Ignition Conditions in Tokamaks," ORNL/TM-9722, Oak Ridge National Laboratory, 1985; "Relative Merits of Size, Field, and Current on Ignited Plasma Performance," ORNL/TM-10365, Oak Ridge National Laboratory, 1987.
- [7] H. C. Howe, "Physics Models in the Tokamak Transport Code PROCTR," ORNL/TM-9537, Oak Ridge National Laboratory, 1985.
- [8] D. Post et al., "Physics Aspects of the Compact Ignition Tokamak," *Phys. Scr.*, vol. T16, pp. 89–106, 1987; J. Sheffield et al., "Physics Guidelines for Compact Ignition Tokamak," *Fusion Technol.*, vol. 10, pp. 481–490, 1986.
- [9] W. A. Houlberg, "Plasma Engineering Assessment of Compact Ignition Experiments," in *Proc. 11th Symposium on Fusion Engineering*, 1985, pp. 50–55; C. E. Singer et al., "Physics of Compact Ignition Tokamak Designs," *ibid.*, pp. 41–49.
- [10] B. A. Trubnikov, "Universal Coefficients for Synchrotron Emission from Plasma Configurations," *Reviews of Plasma Physics*, vol. 7, M. A. Leontovitch, ed., Consultants Bureau, New York, 1979, pp. 345–379.
- [11] S. M. Kaye, "A Review of Energy Confinement and Local Transport Scaling Results in Neutral-Beam-Heated Tokamaks," *Phys. Fluids*, vol. 28, pp. 2327–2343, 1985.
- [12] C. S. Chang and F. L. Hinton, "Effect of Finite Aspect Ratio on the Neoclassical Conductivity in the Banana Regime," *Phys. Fluids*, vol. 25, pp. 1493–1494, 1981.

INTERNAL DISTRIBUTION

- | | | | |
|-------|-----------------|--------|-----------------------------------------------|
| 1. | L. A. Berry | 18. | T. E. Shannon |
| 2. | B. A. Carreras | 19. | J. Sheffield |
| 3. | R. A. Dory | 20-29. | N. A. Uckan |
| 4. | J. L. Dunlap | 30. | T. Uckan |
| 5. | J. D. Galambos | 31-32. | Laboratory Records Department |
| 6. | W. A. Houlberg | 33. | Laboratory Records, ORNL-RC |
| 7-11. | H. C. Howe | 34. | Document Reference Section |
| 12. | J. F. Lyon | 35. | Central Research Library |
| 13. | M. Murakami | 36. | Fusion Energy Division Library |
| 14. | S. L. Painter | 37-38. | Fusion Energy Division
Publications Office |
| 15. | Y-K. M. Peng | 39. | ORNL Patent Office |
| 16. | R. L. Reid | | |
| 17. | M. J. Saltmarsh | | |

EXTERNAL DISTRIBUTION

40. Office of the Assistant Manager for Energy Research and Development, U.S. Department of Energy, Oak Ridge Operations Office, P. O. Box E, Oak Ridge, TN 37831
41. J. D. Callen, Department of Nuclear Engineering, University of Wisconsin, Madison, WI 53706-1687
42. J. F. Clarke, Director, Office of Fusion Energy, Office of Energy Research, ER-50 Germantown, U.S. Department of Energy, Washington, DC 20545
43. R. W. Conn, Department of Chemical, Nuclear, and Thermal Engineering, University of California, Los Angeles, CA 90024
44. S. O. Dean, Fusion Power Associates, Inc., 2 Professional Drive, Suite 249, Gaithersburg, MD 20879
45. H. K. Forsen, Bechtel Group, Inc., Research Engineering, P. O. Box 3965, San Francisco, CA 94105
46. J. R. Gilleland, L-644, Lawrence Livermore National Laboratory, P.O. Box 5511, Livermore, CA 94550
47. R. W. Gould, Department of Applied Physics, California Institute of Technology, Pasadena, CA 91125
48. R. A. Gross, Plasma Research Laboratory, Columbia University, New York, NY 10027

49. D. M. Meade, Princeton Plasma Physics Laboratory, P.O. Box 451, Princeton, NJ 08544
50. M. Roberts, International Programs, Office of Fusion Energy, Office of Energy Research, ER-52 Germantown, U.S. Department of Energy, Washington, DC 20545
51. W. M. Stacey, School of Nuclear Engineering and Health Physics, Georgia Institute of Technology, Atlanta, GA 30332
52. D. Steiner, Nuclear Engineering Department, NES Building, Tibbetts Avenue, Rensselaer Polytechnic Institute, Troy, NY 12181
53. R. Varma, Physical Research Laboratory, Navrangpura, Ahmedabad 380009, India
54. Bibliothek, Max-Planck Institut für Plasmaphysik, Boltzmannstrasse 2, D-8046 Garching, Federal Republic of Germany
55. Bibliothek, Institut für Plasmaphysik, KFA Jülich GmbH, Postfach 1913, D-5170 Jülich, Federal Republic of Germany
56. Bibliothek, KfK Karlsruhe GmbH, Postfach 3640, D-7500 Karlsruhe 1, Federal Republic of Germany
57. Bibliotheque, Centre de Recherches en Physique des Plasmas, Ecole Polytechnique Federale de Lausanne, 21 Avenue des Bains, CH-1007 Lausanne, Switzerland
58. F. Prévot, CEN/Cadarache, Departement de Recherches sur la Fusion Contrôlée, F-13108 Saint-Paul-lez-Durance Cedex, France
59. Bibliothèque, CEN/Cadarache, F-13108 Saint-Paul-lez-Durance Cedex, France
60. Documentation S.I.G.N., Departement de la Physique du Plasma et de la Fusion Contrôlée, Association EURATOM-CEA, Centre d'Etudes Nucléaires, B.P. 85, Centre du Tri, F-38041 Grenoble, France
61. Library, Culham Laboratory, UKAEA, Abingdon, Oxfordshire, OX14 3DB, England
62. Library, JET Joint Undertaking, Abingdon, Oxfordshire, OX14 3EA, England
63. Library, FOM-Instituut voor Plasmafysica, Rijnhuizen, Edisonbaan 14, 3439 MN Nieuwegein, The Netherlands
64. Library, Institute of Plasma Physics, Nagoya University, Chikusa-ku, Nagoya 464, Japan
65. Library, International Centre for Theoretical Physics, P.O. Box 586, I-34100 Trieste, Italy
66. Library, Centro Ricerca Energia Frascati, C.P. 65, I-00044 Frascati (Roma), Italy
67. Library, Plasma Physics Laboratory, Kyoto University, Gokasho, Uji, Kyoto, Japan
68. Plasma Research Laboratory, Australian National University, P.O. Box 4, Canberra, A.C.T. 2601, Australia
69. Library, Japan Atomic Energy Research Institute, Tokai Research Establishment, Tokai, Naka-gun, Ibaraki-ken 311-02, Japan
70. Library, Japan Atomic Energy Research Institute, Naka Research Establishment, Naka-machi, Naka-gun, Ibaraki-ken, Japan
71. G. A. Eliseev, I. V. Kurchatov Institute of Atomic Energy, P. O. Box 3402, 123182 Moscow, U.S.S.R.

72. V. A. Glukhikh, Scientific-Research Institute of Electro-Physical Apparatus, 188631 Leningrad, U.S.S.R.
73. I. Shpigel, Institute of General Physics, U.S.S.R. Academy of Sciences, Ulitsa Vavilova 38, Moscow, U.S.S.R.
74. D. D. Ryutov, Institute of Nuclear Physics, Siberian Branch of the Academy of Sciences of the U.S.S.R., Sovetskaya St. 5, 630090 Novosibirsk, U.S.S.R.
75. V. T. Tolok, Kharkov Physical-Technical Institute, Academical St. 1, 310108 Kharkov, U.S.S.R.
76. Library, Academia Sinica, P.O. Box 3908, Beijing, China (PRC)
77. R. A. Blanken, Experimental Plasma Research Branch, Division of Applied Plasma Physics, Office of Fusion Energy, Office of Energy Research, ER-542, Germantown, U.S. Department of Energy, Washington, DC 20545
78. K. Bol, Princeton Plasma Physics Laboratory, P.O. Box 451, Princeton, NJ 08544
79. R. A. E. Bolton, IREQ Hydro-Quebec Research Institute, 1800 Montee Ste.-Julie, Varennes, P.Q. JOL 2P0, Canada
80. D. H. Crandall, Experimental Plasma Research Branch, Division of Applied Plasma Physics, Office of Fusion Energy, Office of Energy Research, ER-542, Germantown, U.S. Department of Energy, Washington, DC 20545
81. R. L. Freeman, GA Technologies, Inc., P.O. Box 85608, San Diego, CA 92138
82. K. W. Gentle, RLM 11.222, Institute for Fusion Studies, University of Texas, Austin, TX 78712
83. R. J. Goldston, Princeton Plasma Physics Laboratory, P.O. Box 451, Princeton, NJ 08544
84. J. C. Hosea, Princeton Plasma Physics Laboratory, P.O. Box 451, Princeton, NJ 08544
85. S. W. Luke, Division of Confinement Systems, Office of Fusion Energy, Office of Energy Research, ER-55, Germantown, U.S. Department of Energy, Washington, DC 20545
86. E. Oktay, Division of Confinement Systems, Office of Fusion Energy, Office of Energy Research, ER-55, Germantown, U.S. Department of Energy, Washington, DC 20545
87. D. Overskei, GA Technologies, Inc., P.O. Box 85608, San Diego, CA 92138
88. R. R. Parker, Plasma Fusion Center, NW 16-288, Massachusetts Institute of Technology, Cambridge, MA 02139
89. W. L. Sadowski, Fusion Theory and Computer Services Branch, Division of Applied Plasma Physics, Office of Fusion Energy, Office of Energy Research, ER-541, Germantown, U.S. Department of Energy, Washington, DC 20545
90. J. W. Willis, Division of Confinement Systems, Office of Fusion Energy, Office of Energy Research, ER-55, Germantown, U.S. Department of Energy, Washington, DC 20545
91. A. P. Navarro, Division de Fusion, CIEMAT, Avenida Complutense 22, E-28040 Madrid, Spain

92. Laboratory for Plasma and Fusion Studies, Department of Nuclear Engineering, Seoul National University, Shinrim-dong, Gwanak-ku, Seoul 151, Korea
93. M. A. Abdou, School of Engineering and Applied Science, 6288 Boelter Hall, University of California, Los Angeles, CA 90024
94. C. C. Baker, Argonne National Laboratory, 9700 South Cass Avenue, Argonne, IL 60439
95. C. Bolton, Office of Fusion Energy, Office of Energy Research, ER-55 Germantown, U.S. Department of Energy, Washington, DC 20545
96. D. R. Cohn, Plasma Fusion Center, NW 16-140, Massachusetts Institute of Technology, Cambridge, MA 02139
97. B. Coppi, 77 Massachusetts Avenue, Massachusetts Institute of Technology, Cambridge, MA 02139
98. R. C. Davidson, 77 Massachusetts Avenue, Massachusetts Institute of Technology, Cambridge, MA 02139
99. N. A. Davies, Office of Fusion Energy, Office of Energy Research, ER-55 Germantown, U.S. Department of Energy, Washington, DC 20545
100. S. A. Eckstrand, Office of Fusion Energy, Office of Energy Research, ER-55 Germantown, U.S. Department of Energy, Washington, DC 20545
101. A. J. Favale, MS-A0126, Grumman Corporation, P.O. Box 31, Bethpage, NY 11714
102. T. K. Fowler, L-640, Lawrence Livermore National Laboratory, P.O. Box 5511, Livermore, California 94550
103. H. P. Furth, Princeton Plasma Physics Laboratory, P.O. Box 451, Princeton, NJ 08544
104. C. D. Henning, L-640, Lawrence Livermore National Laboratory, P.O. Box 5511, Livermore, California 94550
105. T. R. James, Office of Fusion Energy, Office of Energy Research, ER-55 Germantown, U.S. Department of Energy, Washington, DC 20545
106. R. A. Krakowski, CTR-12, Mail Stop 641, Los Alamos National Laboratory, P.O. Box 1663, Los Alamos, NM 87545
107. G. L. Kulcinski, Room 439, Department of Nuclear Engineering, Engineering Research Building, University of Wisconsin, 1500 Johnson Drive, Madison, WI 53706
108. B. G. Logan, L-644, Lawrence Livermore National Laboratory, P.O. Box 5511, Livermore, California 94550
109. J. A. Maniscalco, R1/2128, TRW Defense and Space Systems, One Space Park, Redondo Beach, CA 90278
110. G. H. Miley, Nuclear Engineering Department, University of Illinois, Urbana, IL 61801
111. D. B. Montgomery, Plasma Fusion Center, NW 16-140, Massachusetts Institute of Technology, Cambridge, MA 02139
112. D. E. Post, Princeton Plasma Physics Laboratory, P.O. Box 451, Princeton, NJ 08544

113. P. H. Rebut, JET Joint Undertaking, Abingdon, Oxon OX14 3EA, England
114. F. L. Ribe, College of Engineering, FL-10, AERL Bldg., University of Washington, Seattle, WA 98195
115. D. Ross, Fusion Research Center, The University of Texas, Austin, TX 78712
116. P. H. Rutherford, Princeton Plasma Physics Laboratory, P.O. Box 451, Princeton, NJ 08544
117. J. A. Schmidt, Princeton Plasma Physics Laboratory, P.O. Box 451, Princeton, NJ 08544
118. R. D. Stambaugh, GA Technologies, Inc., P.O. Box 85608, San Diego, CA 92138
119. P. M. Stone, Office of Fusion Energy, Office of Energy Research, ER-55 Germantown, U.S. Department of Energy, Washington, DC 20545
120. H. Weitzner, Courant Institute of Mathematical Sciences, New York University, 251 Mercer Street, New York, NY 10012
- 121-198. Given distribution as shown in TIC-4500, Magnetic Fusion Energy (Distribution Category UC-20)

